iScience

CellPress
OPEN ACCESS

Article

RQC helical hairpin in Bloom's syndrome helicase regulates DNA unwinding by dynamically intercepting nascent nucleotides

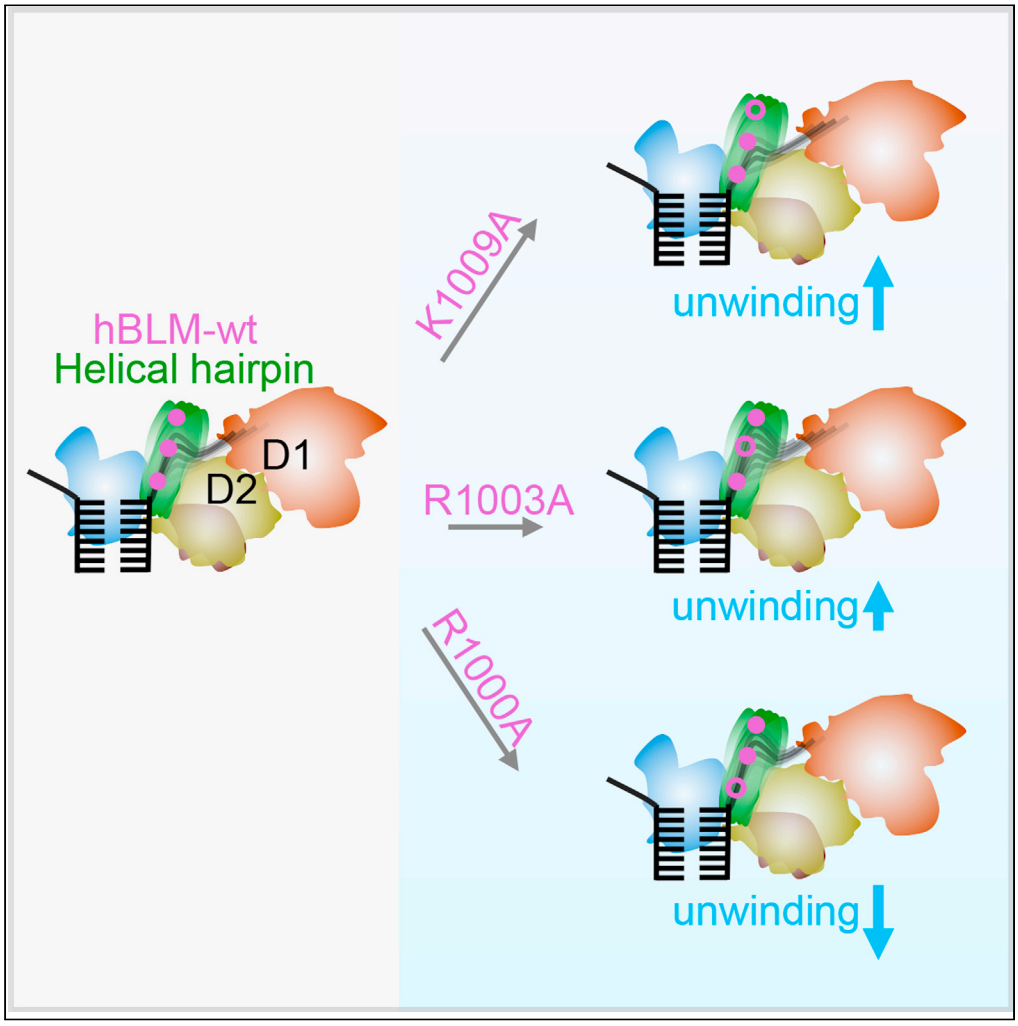

Jianbing Ma, Chunhua Xu, Jinghua Li, ..., Xuguang Xi, Ying Lu, Ming Li

xxi01@ens-cachan.fr (X.X.)
yinglu@iphy.ac.cn (Y.L.)

Highlights

Single-stranded DNA in the DNA-BLM complex is structurally dynamic

Interactions between helical hairpin of BLM and ssDNA are heterogeneous

Single site mutations in the helical hairpin change the conformation of DNA

The helical hairpin regulates DNA unwinding by dynamically intercepting nascent DNA.

Ma et al., iScience 25, 103606
January 21, 2022
https://doi.org/10.1016/j.isci.2021.103606

iScience

CellPress
OPEN ACCESS

Article

RQC helical hairpin in Bloom's syndrome helicase regulates DNA unwinding by dynamically intercepting nascent nucleotides

Jianbing Ma,[1,2,8] Chunhua Xu,[2,8] Jinghua Li,[2] Xi-Miao Hou,[3] Lin-Tai Da,[4] Qi Jia,[1,2,5] Xingyuan Huang,[2,5] Jin Yu,[6] Xuguang Xi,[7,*] Ying Lu,[1,2,5,9,*] and Ming Li[1,2,5]

SUMMARY

The RecQ family of helicases are important for maintenance of genomic integrity. Although functions of constructive subdomains of this family of helicases have been extensively studied, the helical hairpin (HH) in the RecQ-C-terminal domain (RQC) has been underappreciated and remains poorly understood. Here by using single-molecule fluorescence resonance energy transfer, we found that HH in the human BLM transiently intercepts different numbers of nucleotides when it is unwinding a double-stranded DNA. Single-site mutations in HH that disrupt hydrogen bonds and/or salt bridges between DNA and HH change the DNA binding conformations and the unwinding features significantly. Our results, together with recent clinical tests that correlate single-site mutations in HH of human BLM with the phenotype of cancer-predisposing syndrome or Bloom's syndrome, implicate pivotal roles of HH in BLM's DNA unwinding activity. Similar mechanisms might also apply to other RecQ family helicases, calling for more attention to the RQC helical hairpin.

INTRODUCTION

By translocating on single-stranded DNA (ssDNA) in the 3′ to 5′ direction and unwinding double-stranded DNA (dsDNA) (Rada et al., 2015), the RecQ helicases play diverse roles in DNA transactions such as replication (Chappidi et al., 2020; Chu and Hickson, 2009; Delamarre et al., 2020; Shorrocks et al., 2021), recombination (Chu and Hickson, 2009), repair (Adams et al., 2003; Bernstein et al., 2010; Chu and Hickson, 2009; Ferrari et al., 2020; Singh et al., 2012), and telomere maintenance (Bernstein et al., 2010; Chu and Hickson, 2009; Panier et al., 2019). They are highly conserved from bacteria to human and are often called guardians of the genome (Singh et al., 2012). Mutations of the RecQ genes may result in severe genetic disorders in humans such as Werner syndrome (WRN mutated) (Fang et al., 2019; Gray et al., 1997), Bloom's syndrome (BLM mutated) (Goss et al., 2002; Gruber et al., 2002; Yamagata et al., 1998), and Rothmund-Thomson syndrome (RECQ4 mutated) (Hunter, 2008). The other two members, RECQ1 and RECQ5, have not yet been linked to any disease phenotype, but researches have suggested that they are important for genome stability (Singh et al., 2012). The RecQ helicases have three conserved sequence elements: the helicase domain (including two RecA-like domains), the RecQ-C-terminal domain (RQC), and the helicase-and-RNaseD-like-C-terminal domain (HRDC) (Manthei et al., 2015; Morozov et al., 1997). The RQC domain is composed of two elements: a zinc-binding subdomain (ZBD) and a conserved winged-helix (WH) subdomain (Bennett and Keck, 2004; Manthei et al., 2015). ZBD is characterized by a pair of antiparallel α-helices (often called the helical hairpin) and a platform of four α-helices (often called the zinc-binding motif) that ligand a Zn^{2+} ion via four highly conserved cysteine side chains (Swan et al., 2014). In addition to these elements, eukaryotic RecQ proteins often encode N- and C-terminal extensions that confer additional enzymatic activities, sequences that are important for binding to heterologous proteins, and motifs that facilitate proper subcellular localization (Bachrati and Hickson, 2003). The structures and functions of the domains have been intensively investigated (Bennett and Keck, 2004; Chatterjee et al., 2014; Davies et al., 2007; Harami et al., 2013; Newman et al., 2015; Pike et al., 2009; Swan et al., 2014; Wu et al., 2005). However, the helical hairpin in the RQC domain is underappreciated, and its function remains elusive.

Recent clinical tests archived in ClinVar (Landrum et al., 2018) indicated that mutations in the helical hairpin of human BLM (hBLM), such as Arg1000Thr (SCV001179034.2, submitted on Nov 30, 2020; SCV001384683.2,

[1]Songshan Lake Materials Laboratory, Dongguan, Guangdong 523808, China

[2]Beijing National Laboratory for Condensed Matter Physics, Institute of Physics, Chinese Academy of Sciences, Beijing 100190, China

[3]College of Life Sciences, Northwest A&F University, Yangling 712100, Shaanxi, China

[4]Key Laboratory of System Biomedicine (Ministry of Education), Shanghai Center for Systems Biomedicine, Shanghai Jiao Tong University, Shanghai 200240, China

[5]University of Chinese Academy of Sciences, Beijing 100049, China

[6]Department of Physics and Astronomy, Department of Chemistry, NSF-Simons Center for Multiscale Cell Fate Research, University of California, Irvine, CA 92697, USA

[7]LBPA, ENS de Cachan, CNRS, Université Paris-Saclay, Cachan 94235, France

[8]These authors contributed equally

[9]Lead contact

*Correspondence: xxi01@ens-cachan.fr (X.X.), yinglu@iphy.ac.cn (Y.L.)

https://doi.org/10.1016/j.isci.2021.103606

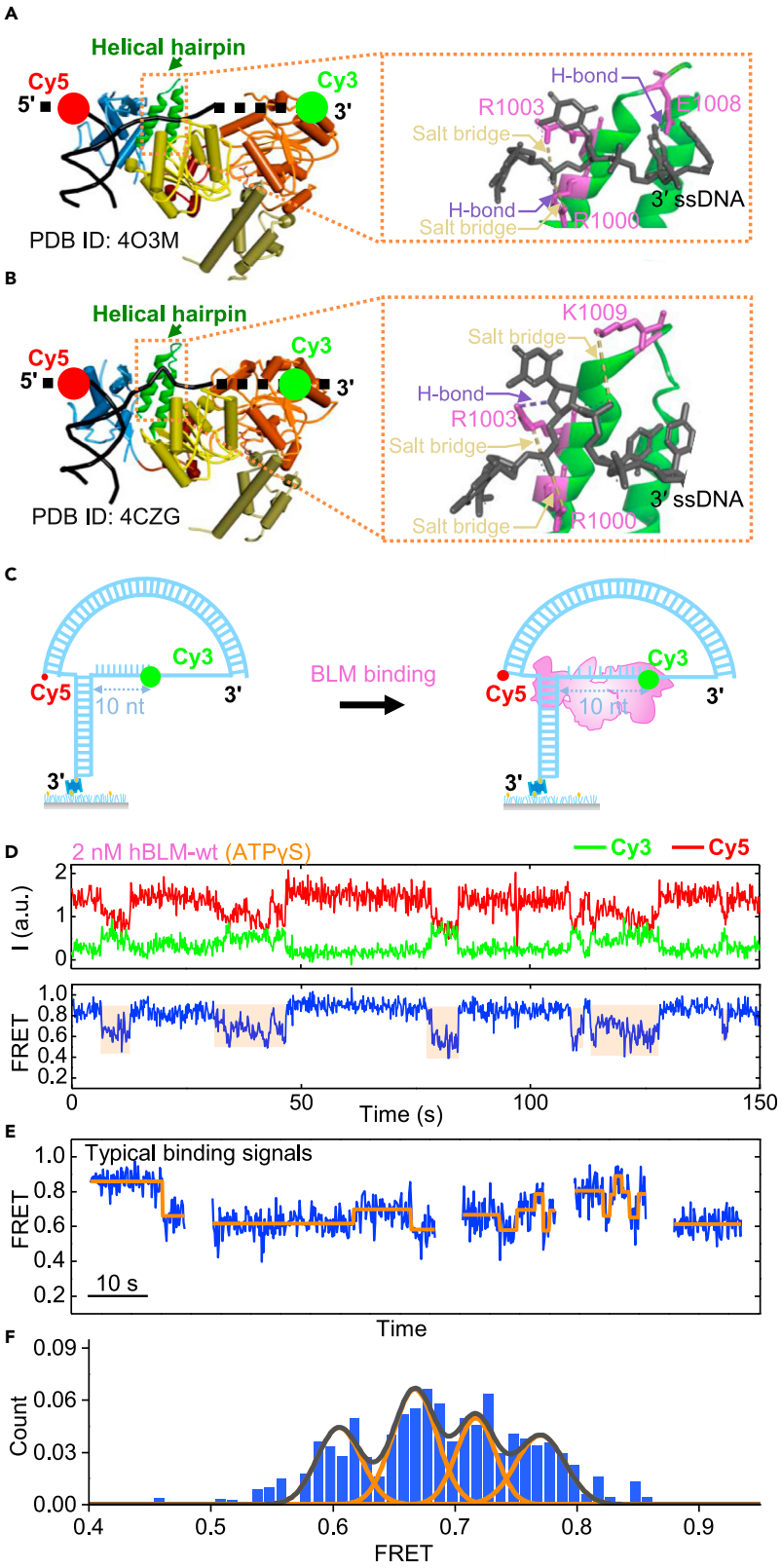
A
Helical hairpin
Cy5
Cy3
5'
3'
PDB ID: 4O3M
H-bond
R1003
K1008
Salt bridge
H-bond
Salt bridge
R1000
3′ ssDNA
B
Helical hairpin
Cy5
Cy3
5'
3'
PDB ID: 4CZG
K1009
Salt bridge
H-bond
R1003
Salt bridge
Salt bridge
R1000
3′ ssDNA
C
Cy3
Cy5
10 nt
3'
3'
BLM binding
Cy3
Cy5
10 nt
3'
3'
D
2 nM hBLM-wt (ATPγS)
Cy3
Cy5
I (a.u.)
FRET
Time (s)
E
Typical binding signals
FRET
10 s
Time
F
Count
FRET

Figure 1. hBLM has multiple DNA binding conformations

(A and B) Two crystal structures of the hBLM-DNA complex (PDB ID: 4O3M and 4CGZ). The zoom-ins display interactions between the helical hairpin and the ssDNA overhang according to the X-ray structures.

(C) A DNA nanotensioner used in the assay. Cy3 was labeled at the 10th nucleotide on the ssDNA overhang, which is elongated upon BLM binding.

(D) A typical FRET trace of hBLM binding to DNA.

(E) Selected DNA binding bursts in the traces show multiple conformations.

(F) Histogram with a multiple peak fitting to the binding signals. The histogram was built from 325 states of 52 traces.

See also Figures S1 and S2.

Jan 07, 2021), Arg1000Ser (SCV000816030.1, submitted on Aug. 29, 2018), Glu1008Lysfs (SCV000486109.1, submitted on Nov. 23, 2016), and Glu1008Val (SCV001413625.2, submitted on Jan 07, 2021) may explain the phenotype of cancer-predisposing syndrome or Bloom's syndrome. These results attracted our attention to the helical hairpin. Structures of the hBLM (Newman et al., 2015; Swan et al., 2014), the human RECQ1 (Pike et al., 2015), and the *Cronobacter sakazakii* RecQ (Manthei et al., 2015) in complex with DNA have been reported. The helical hairpin interacts with the 3′ ssDNA overhangs in all the reported structures. For instance, the charged amino acid residues (R1000, R1003, E1008 and K1009) in the two reported X-ray structures of the hBLM-DNA complex (PDB IDs: 4CGZ and 4O3M) interact with ssDNA via hydrogen bonds and/or salt bridges (Figures 1A and 1B) (Newman et al., 2015; Swan et al., 2014). In 4O3M, R1000 interacts with ssDNA via a hydrogen bond and a salt bridge, E1008 interacts with ssDNA via a hydrogen bond, and R1003 interacts with ssDNA through a salt bridge. By contrast, the hydrogen bonds involving R1000 and E1008 are gone in 4CGZ but a new hydrogen bond is formed between R1003 and ssDNA. Moreover, K1009 is involved with a salt bridge in 4CGZ. More interestingly, there is a prominent difference between the two structures, that is, the ssDNA is straight in 4O3M, whereas it is curved in 4CGZ with an extra nucleotide extruding toward the helical hairpin (Newman et al., 2015; Swan et al., 2014). It seems that the interaction sites tend to shift to the tip of the helical hairpin when a nucleotide extrudes toward the helical hairpin. We wondered if the ssDNA would display more conformations in the complex. If yes, would these conformations affect their dsDNA unwinding activity and potentially correlate with the pathogenic mutations mentioned earlier?

Correlating conformational states to biochemical functions requires the ability to resolve structural dynamics. Single molecule fluorescence resonance energy transfer (smFRET) is becoming a key method for studying such structural dynamics under biologically relevant conditions (Lerner et al., 2018, 2021). Here, we employed smFRET (Lin et al., 2017; Ma et al., 2020; Myong et al., 2005) to investigate dynamic conformations of the ssDNA overhang in the DNA-hBLM complex. To our surprise, we found that the ssDNA overhang binds hBLM with multiple distinct conformations, which can be strongly correlated to the helical hairpin of hBLM. More interestingly, single-site mutations in the helical hairpin regulate the conformations and modulate the DNA unwinding activities significantly.

RESULTS

ssDNA in the DNA-hBLM complex has multiple conformations

We first carried out a DNA binding assay of wild-type hBLM (hBLM-wt). The substrate for hBLM was a double-stranded DNA (dsDNA) with a 30-nt dT ssDNA overhang. In our previous single-turnover stopped-flow assay, we studied hBLM-catalyzed unwinding of a 16-bp dsDNA with a 3′ dT overhang of various lengths (10–40 nt). It turned out that the length of the ssDNA overhang does not change the total time of the ssDNA translocation and the dsDNA unwinding, implying that most of the hBLM molecules bind the ssDNA-dsDNA junction without possible ssDNA translocations (Xu et al., 2012). We adopted a nanotensioner (Lin et al., 2017) to exert tension (~6 pN) on the overhang of the DNA hybrid (Figure 1C). Compared with a forked DNA with free overhangs, the distance between the two fluorescent dyes in the nanotensioner structure is stabilized and increased due to the tension on the overhang (Lin et al., 2017). As a result, the precision of the FRET assay can be improved to resolve distance changes of 1 nt (Lin et al., 2017), which is high enough to reveal distinct states of the DNA binding and unwinding of the helicase. The FRET signal is steady in the absence of the proteins (Figure S1B). Upon addition of hBLM-wt (2 nM) and ATPγS (0.2 mM), the FRET value changes (Figure 1D), indicating binding (in the orange zones) and unbinding events of BLM to the substrate. The time intervals between the orange zones increase with the decreasing of the helicase concentration, whereas the durations of the orange zones are independent of the helicase concentration (Figure S1C and S1D), suggesting that the binding signals were produced by single helicases.

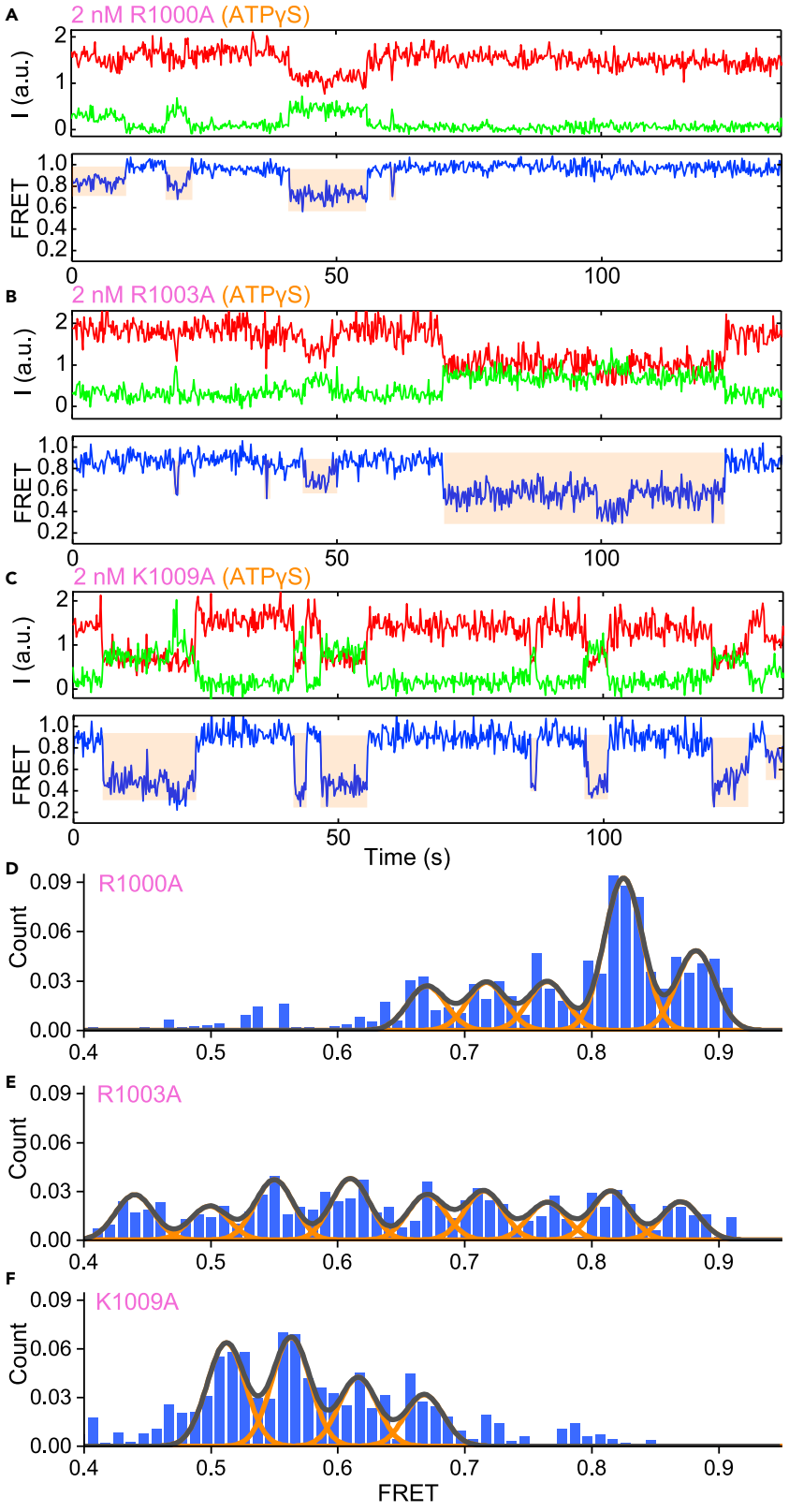
A
2 nM R1000A (ATPγS)
I (a.u.)
FRET
B
2 nM R1003A (ATPγS)
I (a.u.)
FRET
C
2 nM K1009A (ATPγS)
I (a.u.)
FRET
Time (s)
D
R1000A
Count
E
R1003A
Count
F
K1009A
Count
FRET

Figure 2. Single-site mutations of the helical hairpin affect the DNA binding of hBLM

(A–C) Typical single-molecule FRET traces of three hBLM mutants binding to DNA in the presence of ATPγS.

(D–F) Histograms with multiple peak fittings of the binding signals. The histograms were built from 249 states of 53 traces for R1000A, 406 states of 67 traces for R1003A, and 201 states of 49 traces for K1009A, respectively.

See also Figures S3 and S7.

It is noteworthy that the FRET value may vary in a single binding event (Figures 1D and S1C), indicating dynamic conformations of the DNA-BLM complex. We employed an unbiased step-finding algorithm to identify the conformational states, the existence of which can be further checked by the histogram of the states (Blosser et al., 2009; Kerssemakers et al., 2006; Lin et al., 2017; Ma et al., 2020; Myong et al., 2007). A few typical binding events are displayed in Figure 1E. Usually, one to three conformations can be found in one binding event. We collected the states from many binding events and built a histogram of the FRET values. The histogram showed mainly four peaks, indicating different conformational states of the DNA-BLM complex (Figure 1F). Similar binding signals and multiple conformations were also observed in a control assay in the absence of ATPγS (Figure S2). Notably, when Cy3 was labeled at the 10th nucleotide on the overhang, the FRET values for the aforementioned conformations were lower than that without a bound hBLM. This is because the ssDNA in the BLM-DNA complex (PDB ID: 4O3M) is stretched due to strong protein-ssDNA interactions (Figure 1C, right panel). A rough estimation of the Cy3-to-Cy5 distance in the DNA structure used in the measurements yielded a maximum value of about 5.9 nm, which corresponds to a minimum FRET value of about 0.47, assuming that the Förster radius for Cy3 and Cy5 is 5.8 nm and that the 6th–10th nucleotides invisible in the crystal structures interact weakly with the protein. The contribution of partial unwinding of the DNA by BLM would make the FRET value even lower. However, the observed FRET values in Figure 1 are higher than the minimum value we just estimated, indicating that the 10-nt ssDNA segment is shortened as compared with the stretched conformation upon the protein binding. In a structure of the hBLM-DNA complex (PDB ID: 4CGZ), one nucleotide is bent at the helical hairpin (Figure 1B). To explain the reduction in the Cy3-to-Cy5 distance in Figure 1, one may expect that more than one nucleotide could be bent toward the helical hairpin.

Single-site mutations in the helical hairpin modulate the binding conformations

We made single-site mutations at four sites in the helical hairpin. Three mutants (hBLM-R1000A, hBLM-R1003A, and hBLM-K1009A) were purified successfully. The hBLM-E1008A mutant was unstable in solution. Mutations at more than one site resulted in insolubility and degradation of the protein. We performed binding assays similar to that in Figure 1 for the three mutants (Figures 2A–2C and S3). The FRET traces show similar plateaus to that for the hBLM-wt. The histograms of the fitted binding signals also display multiple binding conformations (Figures 2D–2F). However, the mutations changed the statistics of the conformations significantly, implying that the interactions between the helical hairpin and the nucleotides are key to the multiple binding conformations observed earlier.

For the binding conformations of hBLM-R1000A (Figure 2D), it looked that they were shifted to the higher FRET values with respect to those for hBLM-wt (Figure 1F). By contrast, hBLM-K1009A tended to have conformations with lower FRET values than hBLM-wt (Figure 2F). Different from both hBLM-R1000A and hBLM-K1009A, hBLM-R1003A had an obviously wider distribution of conformations than hBLM-wt did (Figure 2E). That is, much more conformations can be found in the histogram for hBLM-R1003A, the number of which was approximately the sum of that for hBLM-R1000A and hBLM-K1009A. We note that a single binding event may, however, display only one to three conformations (Figures 2B and S3B).

Single-site mutations in the helical hairpin modulate the repetitive unwinding pattern

We compared the DNA unwinding activities of hBLM-wt, hBLM-R1000A, hBLM-K1009A, and hBLM-R1003A to gain a deeper insight into the function of the helical hairpin (Figure 3). When Cy3 was labeled too far from the fork, the binding signals would interfere with the unwinding signals (Figures 3B–3E, 3I, 3J, and S4). To ensure effective observation of the signals of the DNA unwinding, Cy3 was moved nearer to the DNA fork. For instance, Cy3 was moved from the 10th to the 6th nucleotide on the overhang for hBLM-wt and hBLM-R1000A (Figure 3F), whereas it was moved to the –third nucleotide for hBLM-K1009A and hBLM-R1003A (Figure 3K). The DNA unwinding signals of 2 nM hBLM at 50 μM ATP were recorded. It turned out that the differently mutated helicases behaved differently. Just like those reported previously (Wang et al., 2015; Yodh et al., 2009), hBLM-wt displayed repetitive unwinding behavior in which the helicase unwinds a short length of dsDNA followed by a rapid re-annealing and re-initiation of unwinding in several

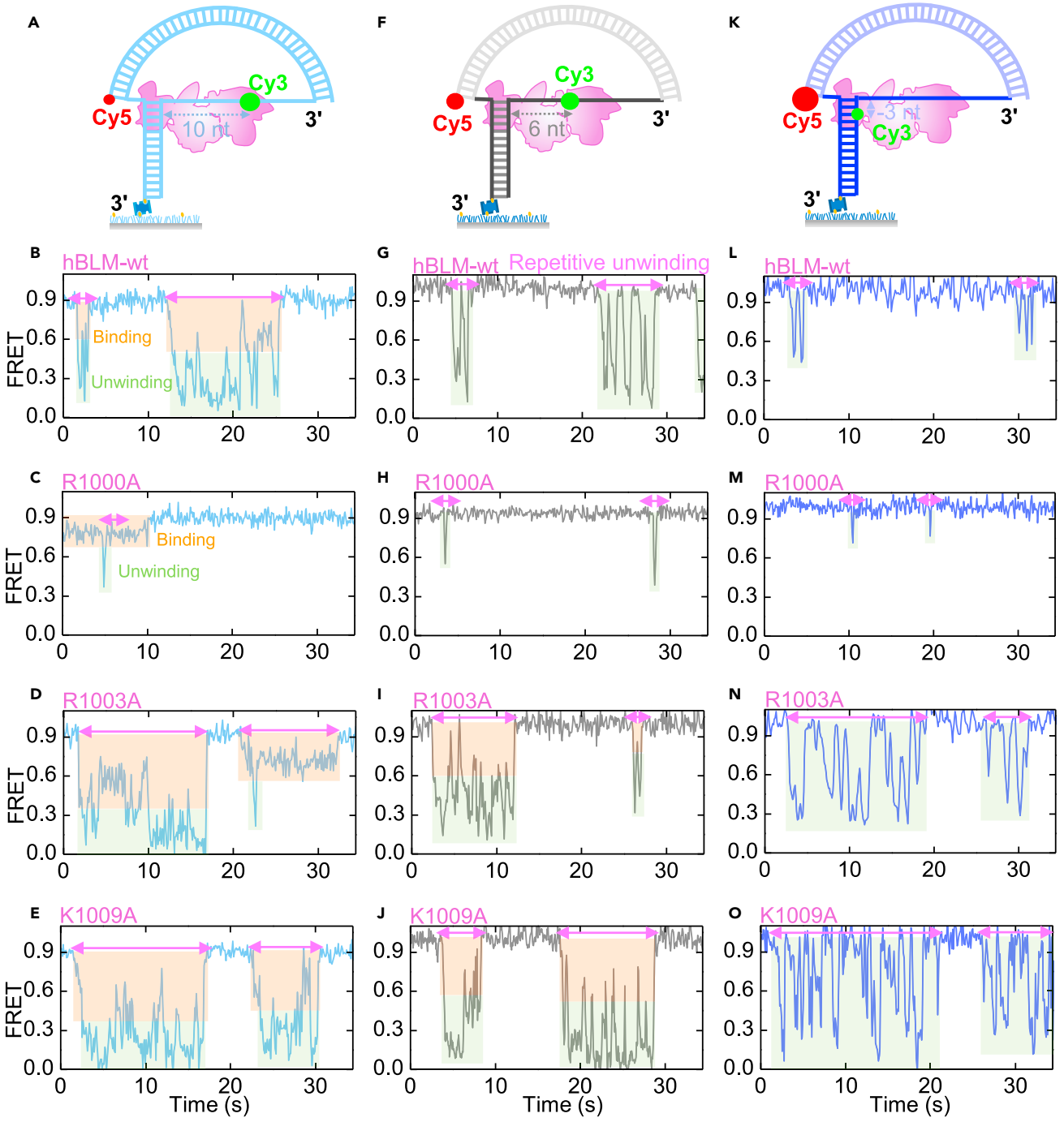

Figure 3. Single-site mutations of the helical hairpin modulate the DNA unwinding pattern

(A–E) Typical unwinding traces obtained by using the DNA construct in which Cy3 was labeled at the 10th nt on the overhang.

(F–J) Typical unwinding traces when Cy3 was at the sixth nt on the overhang.

(K–O) Typical unwinding traces when Cy3 was at −third nt on the overhang. The ATP concentration was 50 μM.

See also Figures S4 and S5.

successions (Figures 3G and L). Similar unwinding behaviors were also observed for hBLM-R1003A (Figure 3N) and hBLM-K1009A (Figure 3O). The average number of repetitive unwinding cycles was 6.9 ± 1.1 for hBLM-R1003A and 10.8 ± 2.2 for hBLM-K1009A (Figure S5), which are larger than the average

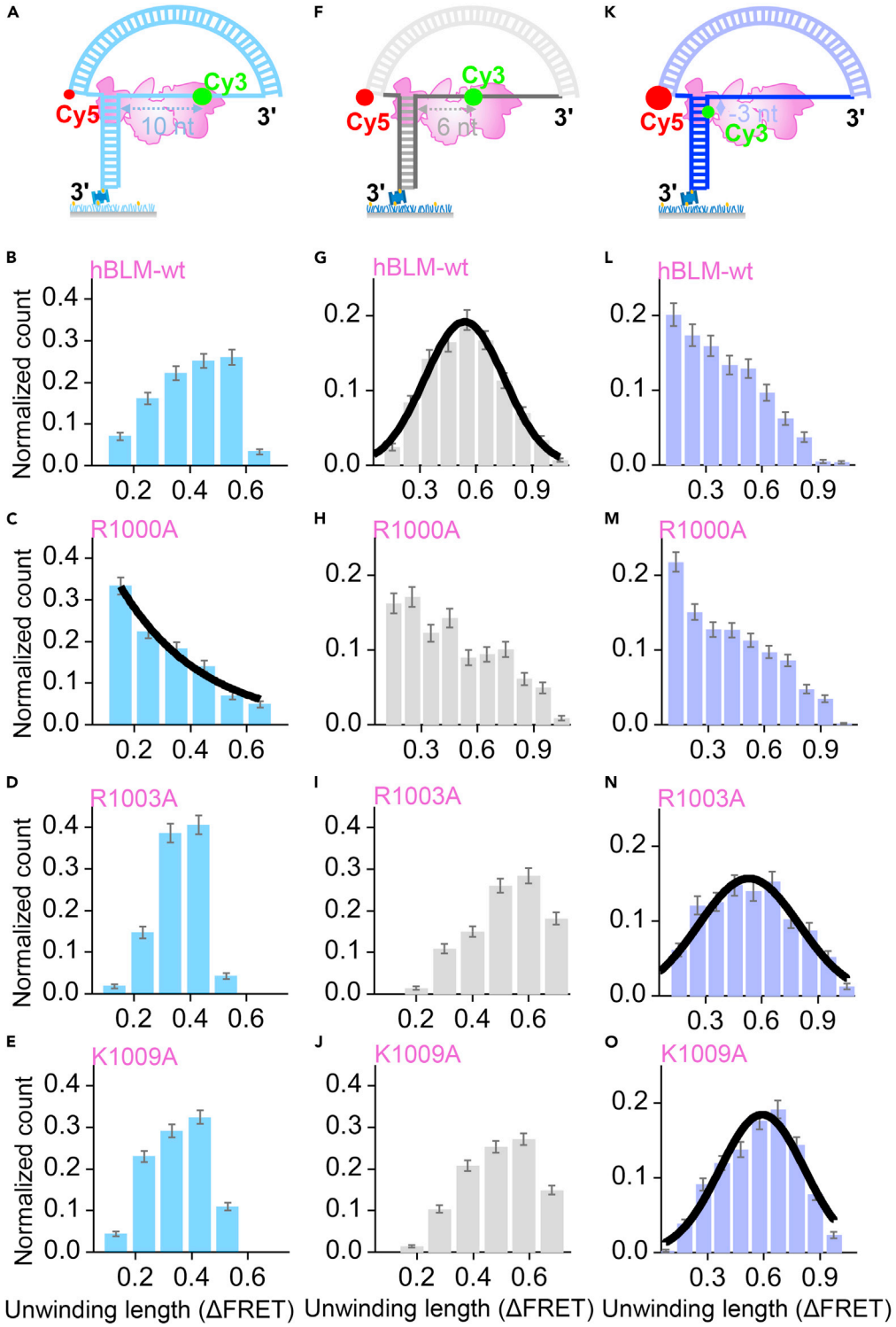

Figure 4. Single-site mutations at the helical hairpin modulate the DNA unwinding length

(A–E) Histograms of the DNA unwinding length in terms of ΔFRET for the four hBLM helicases when Cy3 was labeled at the 10th nt on the overhang.

(F–J) Histograms when Cy3 was labeled at the sixth nt.

(K–O) Histograms when Cy3 was labeled at the −third nt. The start positions of the unwinding bursts (the green boxes) were estimated to be at the ends of the binding signals (the orange boxes). The error bars are proportional to the square root of the number of points for each bin. The number of bursts used in the statistics were 782–1,330. The corresponding number of traces were 383–564 for R1000A and 81–130 for other mutants.

number of repetitive unwinding cycles for hBLM-wt (3.2 ± 0.4) (Figures 3L and S5). By contrast, almost only single unwinding bursts were observable for hBLM-R1000A (Figures 3H and 3M), indicating the peculiarity of this mutation. Although the mutations of R1003A and K1009A only quantitatively changed the unwinding features, the pathogenic mutation of R1000A changed the unwinding features qualitatively.

Single-site mutations in the helical hairpin modulate distribution of the unwinding length

It was previously reported that hBLM-wt unwinds a preferred length of DNA. That is, the distribution of unwinding lengths has a peak (Yodh et al., 2009). This unwinding mode was proposed to have a function in the heteroduplex rejection during early stages of the homologous recombination (Yodh et al., 2009). In order to check whether the single-point mutations would affect this unwinding mode, we constructed statistical distributions of the unwinding lengths in terms of values of ΔFRET (Figure 4). Because the range of reliable FRET signals is limited to 0.2–0.8, we found that only four histograms are effective, namely, Figures 4C, 4G, 4N, and 4O. The other histograms cover only a part of the unwinding signals. It turned out that the histograms of hBLM-wt, hBLM-R1003A, and hBLM-K1009A each displayed a peak. By contrast, the histogram of hBLM-R1000A (Figure 4C) did not have a peak. Rather, it followed an exponential decay. This histogram was built from the traces as the one shown in Figure 3C, in which the unwinding signals can be readily distinguished from the binding signals. By comparing the peak for hBLM-wt in Figure 4G with the ones in Figure 4N for hBLM-R1003A and Figure 4O for hBLM-K1009A, one can conclude that the unwinding lengths of hBLM-R1003A and hBLM-K1009A were at least about 9-nt longer than that of the hBLM-wt because the peak positions were all around 0.6, but the labeling position was at 6 nt in Figure 4F, whereas it was at −3 nt in Figure 4K. A similar argument supports the conclusion that the mean unwinding length of hBLM-R1000A was much shorter than that of hBLM-wt.

DNAs in the WRN-DNA and RecQ-DNA complexes also have multiple conformations

To check whether the multiple binding conformations are also observable for other RecQ helicases, we performed similar binding assays on the *Gallus gallus* WRN and the *Escherichia coli* RecQ (Figure S6). We first used the same DNA substrates as that in Figures 1 and 2 in the binding assay and found that the binding signals were concentrated in the very high FRET region so that it was not easy to distinguish different binding conformations (Figure S6A). The FRET values were much higher than that when hBLM-wt was binding on the same DNA. More binding conformations could be seen when Cy3 was moved from the 10th to the 14th nucleotide on the ssDNA overhang (Figure S6B), indicating that ssDNA in the both helicase-DNA complexes also have multiple conformations. We are currently not able to explain the difference among the bindings of WRN, RecQ and BLM. Two plausible sources may contribute to the difference: (1) the ssDNA interacts with the helical hairpin at different sites in the three helicases; and (2) the sizes and structures of the helical hairpins are different.

DISCUSSION

We observed in this work various binding conformations of ssDNA in the DNA-BLM complex (Figure 1). The binding conformations were further correlated to the helical hairpin in the protein because mutations at the helical hairpin (R1000A, R1003A and K1009A) changed the conformations (Figure 2). The mutations also changed significantly the DNA unwinding features of the helicase (Figures 3 and 4). Enlightened by the two crystal structures of the hBLM-DNA complex (Figures 1A and 1B) (Newman et al., 2015; Swan et al., 2014), we could propose a simple model in which the helical hairpin in BLM transiently intercepts different numbers of nucleotides when it is unwinding a double-stranded DNA (Figure 5). The K1009 residue is near the tip of the helical hairpin, i.e., distal to the surface of the D2 domain of hBLM. Strong interaction between the K1009 site and ssDNA may attract more nucleotides to the helical hairpin. The mutation-induced weakening of the interaction renders the ssDNA hard to extrude as far as it may do in hBLM-wt. Hence the mean Cy3-Cy5 distance in hBLM-K1009A is longer than that in hBLM-wt (Figure 5), thereby the binding FRET values of hBLM-K1009A (Figure 2E) is lower than that of hBLM-wt (Figure 1F). By contrast, the R1000 residue is proximal to the surface of the D2 domain of hBLM. The ssDNA in hBLM-R1000A may tend to extrude further because the mutation of R1000A weakens the ssDNA-R1000 interaction so that it may not be

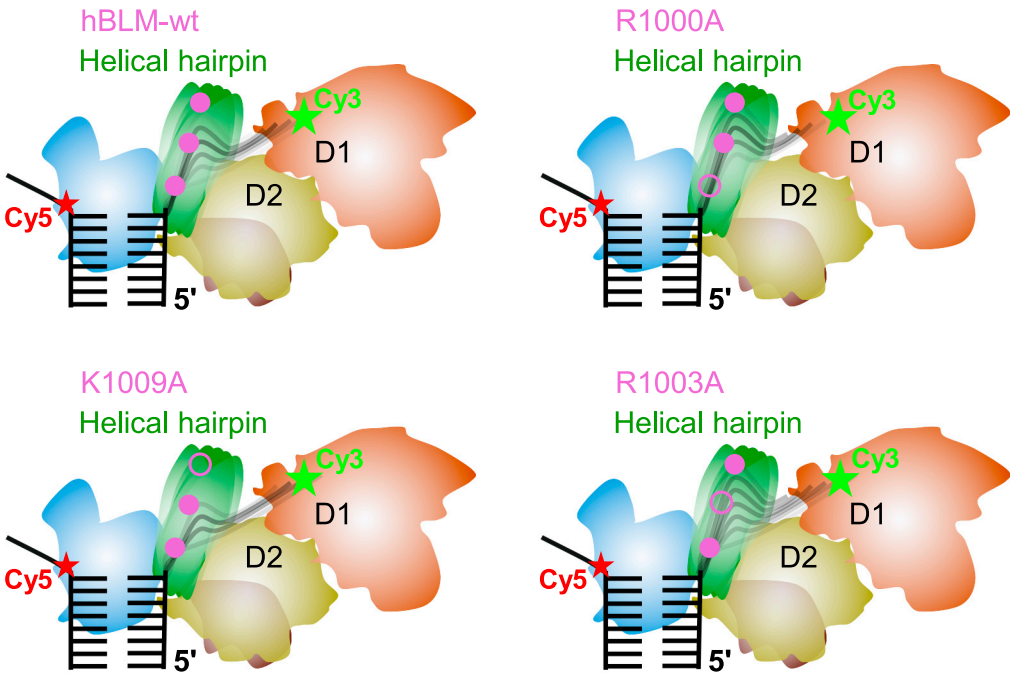

Figure 5. A model of interception of nascent nucleotides by the helical hairpin during DNA unwinding by different hBLM mutants

The DNA-interaction sites (filled cycles) in the helical hairpin affect the interception pattern and hence the binding and unwinding mode. The mutations are marked by open circles. The two RecA-like domains are denoted as D1 and D2. The dyes were labeled on the DNA.

constrained near to the surface of the D2 domain. The three strong interaction sites are all there in hBLM-wt. Therefore, in average, the binding conformations tend to populate at positions with middle FRET values (Figure 1F). The R1003 residue is located between K1009 and R1000 in the helical hairpin. Consistently, when the R1003 site is mutated, the conformations are distributed more widely (Figure 2F).

Many RecQ helicases including hBLM (Yodh et al., 2009), *Escherichia coli* RecQ (Haramia et al., 2017; Lin et al., 2017), human WRN (Lee et al., 2018), and *Arabidopsis thaliana* RecQ2 and RecQ3 (Klaue et al., 2013) display repetitive unwinding activity, which was proposed to play a key role in the biological functions of the helicases, for example, to process stalled replication forks, to eliminate potentially deleterious recombination intermediates, and to strip off other DNA binding proteins during replication fork repair and homologous recombination (Haramia et al., 2017; Klaue et al., 2013; Lee et al., 2018; Lin et al., 2017; Yodh et al., 2009). It was also reported that hBLM has a preferred unwinding length, which may have a function in the heteroduplex rejection during early stages of the homologous recombination (Yodh et al., 2009). Our results showed that the mutations in the helical hairpin changed the unwinding pattern of hBLM (Figures 3 and 4). We note that the average binding durations of the mutants were comparable with that of BLM-wt (Figure S7), suggesting that the modulation to the unwinding pattern was not due to the change of the binding time. Indeed, as an example, one sees in Figure 3C only a single short-time unwinding burst along with a long-time binding signal. It seems that the average number of nucleotides intercepted by the helical hairpin (Figures 1 and 2), the average repetitive unwinding cycle (Figure 3), and the preferred unwinding length (Figure 4) are all correlated to each other. Our data suggest that the unwinding activity of BLM is significantly reduced when more nascent nucleotides are intercepted by the helical hairpin. For instance, the helical hairpin in hBLM-R1000A intercepts the longest length of nucleotides in average, and the corresponding repetitive cycle/unwinding lengths are the fewest/shortest. This is in accordance with the inch-worm mechanism of the translocation of non-ring-shaped helicases along ssDNA, in which the helicases move by alternating affinities between the RecA-like domains (D1 and D2) and the ssDNA at different stages of the ATP hydrolysis cycle (Lohman et al., 2008; Velankar et al., 1999). When the ssDNA was detached from the two RecA-like domains by the helical hairpin, the translocation of the helicase along the ssDNA would be significantly hindered. We made four single-site mutations in the helical hairpin and

found that two of the mutations are peculiar. The hBLM-E1008A mutant was unstable in solution, and the unwinding activity of hBLM-R1000A was significantly reduced, which may be phenomenologically correlated to the pathogenic mutations at R1000 and E1008. On the other hand, the mutations at R1003 and K1009 resulted in higher unwinding activity. However, the enhanced unwinding activity might also have some negative effects because it was pointed out that a too high unwinding activity may inhibit the heteroduplex rejection during early stages of the homologous recombination (Yodh et al., 2009).

In summary, we observed that the nascent nucleotides in the DNA-hBLM complex are dynamically intercepted by the helical hairpin of the helicase. Single-site mutations in the helical hairpin have important impacts on the conformations of the nascent ssDNA. The mutations also result in abnormal changes of the unwinding features of the helicase. Similar binding conformations were also observed in the binding assays of two RecQ family helicases, i.e., WRN and RecQ. Because the helical hairpin is the most understudied subdomain in the RecQ family of helicases and because recent clinical tests archived in ClinVar (Landrum et al., 2018) indicated that some mutations in the helical hairpin of hBLM may explain the phenotype of cancer-predisposing syndrome or Bloom's syndrome, our results should inspire more interests in the RQC helical hairpins.

Limitations of the study

This study observed the dynamic conformations of DNA induced by the helical hairpin in the human Bloom's syndrome helicase. The impact of mutations of the helical hairpin on DNA binding and unwinding demonstrated its key roles in functional regulations. We noticed that, although the mutations of R1003A and K1009A only quantitatively changed the unwinding features, the pathogenic mutation of R1000A changed the unwinding features qualitatively. Further studies are necessary to see if the mutations affect the *in vivo* functions of the BLM helicases. In addition, the roles of the helical hairpin may not be similar for other RecQ helicases.

STAR★METHODS

Detailed methods are provided in the online version of this paper and include the following:

- KEY RESOURCES TABLE
- RESOURCE AVAILABILITY
  - Lead contact
  - Materials availability
  - Data and code availability
- EXPERIMENTAL MODEL AND SUBJECT DETAILS
  - E. coli strains for *in vitro* studies
- METHOD DETAILS
  - Protein expression and purification
  - DNA constructs and annealing procedures
  - Single-molecule FRET assay
- QUANTIFICATION AND STATISTICAL ANALYSIS

SUPPLEMENTAL INFORMATION

Supplemental information can be found online at https://doi.org/10.1016/j.isci.2021.103606.

ACKNOWLEDGMENTS

This work was supported by the National Natural Science Foundation of China [Grant Nos. 12090051, 11834018, and 12022409], the CAS Strategic Priority Research Program (Grant No. XDB37000000), the CAS Key Research Program of Frontier Sciences [Grant Nos. QYZDJ-SSW-SYS014 and ZDBS-LY-SLH015], and the Youth Innovation Promotion Association of CAS [No. 2017015]. We thank Haihong Li for assistance about protein purification.

AUTHOR CONTRIBUTIONS

J.M. and C.X. performed the experiments; C.X. and J.M. designed and made the DNA constructs; J.M., Y.L. and M.L. performed the data analysis; L.T.D., J.Y., J.L., Q.J., and XY.H. assisted with some experiments and

data analysis; X.X. and XM.H. expressed and purified the proteins; Y.L., M.L., and X.X. designed the research; Y.L., M.L., X.X., and J.M. wrote the manuscript.

DECLARATION OF INTERESTS

The authors declare no competing interests.

Received: July 7, 2021
Revised: November 3, 2021
Accepted: December 8, 2021
Published: January 21, 2022

REFERENCES

Adams, M.D., McVey, M., and Sekelsky, J.J. (2003). *Drosophila* BLM in double-strand break repair by synthesis-dependent strand annealing. Science *29*, 265–267.

Bachrati, C.Z., and Hickson, I.D. (2003). RecQ helicases: suppressors of tumorigenesis and premature aging. Biochem. J. *374*, 577–606.

Bennett, R.J., and Keck, J.L. (2004). Structure and function of RecQ DNA helicases. Crit. Rev. Biochem. Mol. Biol. *39*, 79–97.

Bernstein, K.A., Gangloff, S., and Rothstein, R. (2010). The RecQ DNA helicases in DNA repair. Annu. Rev. Genet. *44*, 393–417.

Blosser, T.R., Yang, J.G., Stone, M.D., Narlikar, G.J., and Zhuang, X. (2009). Dynamics of nucleosome remodelling by individual ACF complexes. Nature *462*, 1022–1027.

Chappidi, N., Nascakova, Z., Boleslavska, B., Zellweger, R., Isik, E., Andrs, M., Menon, S., Dobrovolna, J., Pogliano, C.B., Matos, J., et al. (2020). Fork cleavage-religation cycle and active transcription mediate replication restart after fork stalling at Co-transcriptional R-loops. Mol. Cell *77*, 528–541.

Chatterjee, S., Zagelbaum, J., Savitsky, P., Sturzenegger, A., Huttner, D., Janscak, P., Hickson, I.D., Gileadi, O., and Rothenberg, E. (2014). Mechanistic insight into the interaction of BLM helicase with intra-strand G-quadruplex structures. Nat. Commun. *5*, 5556.

Chu, W.K., and Hickson, I.D. (2009). RecQ helicases: multifunctional genome caretakers. Nat. Rev. Cancer *9*, 644–654.

Davies, S.L., North, P.S., and Hickson, I.D. (2007). Role for BLM in replication-fork restart and suppression of origin firing after replicative stress. Nat. Struct. Mol. Biol. *14*, 677–679.

Delamarre, A., Barthe, A., Saint-Andre, C.d.l.R., Luciano, P., Forey, R., Padioleau, I., Skrzypczak, M., Ginalski, K., Geli, V., Pasero, P., et al. (2020). MRX increases chromatin accessibility at stalled replication forks to promote nascent DNA resection and cohesin loading. Mol. Cell *77*, 395–410.

Fang, E.F., Hou, Y., Lautrup, S., Jensen, M.B., Yang, B., SenGupta, T., Caponio, D., Khezri, R., Demarest, T.G., Aman, Y., et al. (2019). NAD^+ augmentation restores mitophagy and limits accelerated aging in Werner syndrome. Nat. Commun. *10*, 5284.

Ferrari, M., Rawal, C.C., Lodovichi, S., Vietri, M.Y., and Pellicioli, A. (2020). Rad9/53BP1 promotes DNA repair via crossover recombination by limiting the Sgs1 and Mph1 helicases. Nat. Commun. *11*, 3181.

Goss, K.H., Risinger, M.A., Kordich, J.J., Sanz, M.M., Straughen, J.E., Slovek, L.E., Capobianco, A.J., German, J., Boivin, G.P., and Groden, J. (2002). Enhanced tumor formation in mice heterozygous for Blm mutation. Science *297*, 2051–2053.

Gray, M.D., Shen, J.-C., Kamath-Loeb, A.S., Blank, A., Sopher, B.L., Martin, G.M., Oshima, J., and Loeb, L.A. (1997). The Werner syndrome protein is a DNA helicase. Nat. Genet. *17*, 100–103.

Gruber, S.B., Ellis, N.A., Scott, K.K., Almog, R., Kolachana, P., Bonner, J.D., Kirchhoff, T., Tomsho, L.P., Nafa, K., Pierce, H., et al. (2002). BLM heterozygosity and the risk of colorectal cancer. Science *297*, 2013.

Guo, R.B., Rigolet, P., Zargarian, L., Fermandjian, S., and Xi, X.G. (2005). Structural and functional characterizations reveal the importance of a zinc binding domain in Bloom's syndrome helicase. Nucleic Acids Res. *33*, 3109–3124.

Harami, G.M., Gyimesi, M., and Kovács, M. (2013). From keys to bulldozers: expanding roles for winged helix domains in nucleic-acid-binding proteins. Trends Biochem. Sci. *38*, 364–371.

Haramia, G.M., Seolb, Y., In, J., Ferencziová, V., Martina, M., Gyimesi, M., Sarlós, K., Kovács, Z.J., Nagy, N.T., Sun, Y., et al. (2017). Shuttling along DNA and directed processing of D-loops by RecQ helicase support quality control of homologous recombination. Proc. Natl. Acad. Sci. U S A *114*, E466–E475.

Hunter, N. (2008). The RecQ DNA helicases: jacks-of-all-trades or master-tradesmen? Cell Res. *18*, 328–330.

Karow, J.K., Chakraverty, R.K., and Hickson, I.D. (1997). The Bloom's syndrome gene product is a 3′-5′ DNA helicase. J. Biol. Chem. *272*, 30611–30614.

Kerssemakers, J.W., Munteanu, E.L., Laan, L., Noetzel, T.L., Janson, M.E., and Dogterom, M. (2006). Assembly dynamics of microtubules at molecular resolution. Nature *442*, 709–712.

Klaue, D., Kobbe, D., Kemmerich, F., Kozikowska, A., Puchta, H., and Seidel, R. (2013). Fork sensing and strand switching control antagonistic activities of RecQ helicases. Nat. Commun. *4*, 2024.

Landrum, M.J., Lee, J.M., Benson, M., Brown, G.R., Chao, C., Chitipiralla, S., Gu, B., Hart, J., Hoffman, D., Jang, W., et al. (2018). ClinVar: improving access to variant interpretations and supporting evidence. Nucleic Acids Res. *46*, D1062–D1067.

Lee, M., Shin, S., Uhm, H., Hong, H., Kirk, J., Hyun, K., Kulikowicz, T., Kim, J., Ahn, B., Bohr, V.A., et al. (2018). Multiple RPAs make WRN syndrome protein a superhelicase. Nucleic Acids Res. *46*, 4689–4698.

Lerner, E., Barth, A., Hendrix, J., Ambrose, B., Birkedal, V., Blanchard, S.C., Borner, R., Sung Chung, H., Cordes, T., Craggs, T.D., et al. (2021). FRET-based dynamic structural biology: challenges, perspectives and an appeal for open-science practices. eLife *10*, e60416.

Lerner, E., Cordes, T., Ingargiola, A., Alhadid, Y., Chung, S., Michalet, X., and Weiss, S. (2018). Toward dynamic structural biology: two decades of single-molecule Förster resonance energy transfer. Science *359*, eaan1133.

Lin, W., Ma, J., Nong, D., Xu, C., Zhang, B., Li, J., Jia, Q., Dou, S., Ye, F., Xi, X., et al. (2017). Helicase stepping investigated with one-nucleotide resolution fluorescence resonance Energy transfer. Phys. Rev. Lett. *119*, 138102.

Lohman, T.M., Tomko, E.J., and Wu, C.G. (2008). Non-hexameric DNA helicases and translocases: mechanisms and regulation. Nat. Rev. Mol. Cell Biol. *9*, 391–401.

Ma, J., Chen, Z., Xu, C., Huang, X., Jia, Q., Zou, Z., Mi, C., Ma, D., Lu, Y., Zhang, H., et al. (2020). Dynamic structural insights into the molecular mechanism of DNA unwinding by the bacteriophage T7 helicase. Nucleic Acids Res. *48*, 3156–3164.

Manthei, K.A., Hill, M.C., Burke, J.E., Butcher, S.E., and Keck, J.L. (2015). Structural mechanisms of DNA binding and unwinding in bacterial RecQ helicases. Proc. Natl. Acad. Sci. U S A *112*, 4292–4297.

Morozov, V., Mushegian, A.R., Koonin, E.V., and Bork, P. (1997). A putative nucleic acid-binding domain in Bloom's and Werner's syndrome helicases. Trends Biochem. Sci. *22*, 417–418.

Myong, S., Bruno, M.M., Pyle, A.M., and Ha, T. (2007). Spring-loaded mechanism of DNA unwinding by hepatitis C virus NS3 helicase. Science *317*, 513–516.

Myong, S., Rasnik, I., Joo, C., Lohman, T.M., and Ha, T. (2005). Repetitive shuttling of a motor protein on DNA. Nature *437*, 1321–1325.

Newman, J.A., Savitsky, P., Allerston, C.K., Bizard, A.H., Özer, Ö., Sarlós, K., Liu, Y., Pardon, E., Steyaert, J., Hickson, I.D., et al. (2015). Crystal structure of the Bloom's syndrome helicase indicates a role for the HRDC domain in conformational changes. Nucleic Acids Res. *43*, 5221–5235.

Panier, S., Maric, M., Hewitt, G., Mason-Osann, E., Gali, H., Dai, A., Labadorf, A., Guervilly, J.H., Ruis, P., Segura-Bayona, S., et al. (2019). SLX4IP antagonizes promiscuous BLM activity during ALT maintenance. Mol. Cell *76*, 27–43.

Pike, A.C., Gomathinayagam, S., Swuec, P., Berti, M., Zhang, Y., Schnecke, C., Marino, F., Delft, F.V., Renault, L., Costa, A., et al. (2015). Human RECQ1 helicase-driven DNA unwinding, annealing, and branch migration: insights from DNA complex structures. Proc. Natl. Acad. Sci. U S A *112*, 4286–4291.

Pike, A.C., Shrestha, B., Popuri, V., Burgess-Brown, N., Muzzolini, L., Costantini, S., Vindigni, A., and Gileadi, O. (2009). Structure of the human RECQ1 helicase reveals a putative strand-separation pin. Proc. Natl. Acad. Sci. U S A *106*, 1039–1044.

Rada, B., Forgeta, A.L., Baskinb, R.J., and Kowalczykowski, S.C. (2015). Single-molecule visualization of RecQ helicase reveals DNA melting, nucleation, and assembly are required for processive DNA unwinding. Proc. Natl. Acad. Sci. U S A *112*, E6852–E6861.

Roy, R., Hohng, S., and Ha, T. (2008). A practical guide to single-molecule FRET. Nat. Methods *5*, 507–516.

Shorrocks, A.K., Jones, S.E., Tsukada, K., Morrow, C.A., Belblidia, Z., Shen, J., Vendrell, I., Fischer, R., Kessler, B.M., and Blackford, A.N. (2021). The Bloom syndrome complex senses RPA-coated single-stranded DNA to restart stalled replication forks. Nat. Commun. *12*, 585.

Singh, D.K., Ghosh, A.K., Croteau, D.L., and Bohr, V.A. (2012). RecQ helicases in DNA double strand break repair and telomere maintenance. Mutat. Res. *736*, 15–24.

Swan, M.K., Legris, V., Tanner, A., Reaper, P.M., Vial, S., Bordas, R., Pollard, J.R., Charlton, P.A., Golec, J.M.C., and Bertrand, J.A. (2014). Structure of human Bloom's syndrome helicase in complex with ADP and duplex DNA. Acta Crystallogr. D Biol. Crystallogr. *70*, 1465–14675.

Teng, F.Y., Wang, T.T., Guo, H.L., Xin, B.G., Sun, B., Dou, S.X., Xi, X.G., and Hou, X.M. (2020). The HRDC domain oppositely modulates the unwinding activity of E. coli RecQ helicase on duplex DNA and G-quadruplex. J. Biol. Chem. *295*, 17646–17658.

Velankar, S.S., Soultanas, P., Dillingham, M.S., Subramanya, H.S., and Wigley, D.B. (1999). Crystal structures of complexes of PcrA DNA helicase with a DNA substrate indicate an inchworm mechanism. Cell *97*, 75–84.

Wang, S., Qin, W., Li, J.H., Lu, Y., Lu, K.Y., Nong, D.G., Dou, S.X., Xu, C.H., Xi, X.G., and Li, M. (2015). Unwinding forward and sliding back: an intermittent unwinding mode of the BLM helicase. Nucleic Acids Res. *43*, 3736–3746.

Wu, L., Chan, K.L., Ralf, C., Bernstein, D.A., Garcia, P.L., Bohr, V.A., Vindigni, A., Janscak, P., Keck, J.L., and Hickson, I.D. (2005). The HRDC domain of BLM is required for the dissolution of double Holliday junctions. EMBO J. *24*, 2679–2687.

Wu, W.Q., Hou, X.M., Zhang, B., Fossé, P., René, B., Mauffret, O., Li, M., Dou, S.X., and Xi, X.G. (2017). Single-molecule studies reveal reciprocating of WRN helicase core along ssDNA during DNA unwinding. Sci. Rep. *7*, 43954.

Xu, Y.N., Bazeille, N., Ding, X.Y., Lu, X.M., Wang, P.Y., Bugnard, E., Grondin, V., Dou, S.X., and Xi, X.G. (2012). Multimeric BLM is dissociated upon ATP hydrolysis and functions as monomers in resolving DNA structures. Nucleic Acids Res. *40*, 9802–9814.

Xu, H.Q., Deprez, E., Zhang, A.H., Tauc, P., Ladjimi, M.M., Brochon, J.C., Auclair, C., and Xi, X.G. (2003). The *Escherichia coli* RecQ helicase functions as a monomer. J. Biol. Chem. *278*, 34925–34933.

Yamagata, K., Kato, J.-i., Shimamoto, A., Goto, M., Furuichi, Y., and Ikeda, H. (1998). Bloom's and Werner's syndrome genes suppress hyperrecombination in *yeast sgs1* mutant: implication for genomic instability in human diseases. Proc. Natl. Acad. Sci. U S A *95*, 8733–8738.

Yodh, J.G., Stevens, B.C., Kanagaraj, R., Janscak, P., and Ha, T.J. (2009). BLM helicase measures DNA unwound before switching strands and hRPA promotes unwinding reinitiation. EMBO J. *28*, 405–416.

STAR★METHODS

KEY RESOURCES TABLE

REAGENT or RESOURCE	SOURCE	IDENTIFIER
Bacterial and virus strains		
E. Coli BL21(DE3) Chemically Competent Cells	(Xu et al., 2003)	CMC0014-20X40UL
Chemicals, peptides, and recombinant proteins		
Glucose Oxidase from Aspergillus niger	Sigma-Aldrich	Cat#BCCB3207
Catalase from bovine liver	Sigma-Aldrich	Cat#SLBW1912
Trolox	Sigma-Aldrich	Cat#BCBW5446
M-PEG-SVA	Laysan Bio, Inc.	Cat#154-82
Biotin-PEG-SVA	Laysan Bio, Inc.	Cat#155-23
Critical commercial assays		
Deposited data		
Raw data	This paper	Mendeley Data: https://doi.org/10.17632/p7tbm4xgsz.1
Oligonucleotides		
Up: **Cy5**-AAACTCACCA TGAAGCGTTT CACTAATGGG CGTGGCTTCT GGTGCATGCT GAAACTCTAC	Sangon Biotech Co., Ltd	N/A
Down 1: GACCTGTACA TGTCCGTCAG CA(**T-Cy3**)CCTTTTT TTTTTTTTT TTTTTTTTT TTTTTGTAGA GTTTCAGCAT GCACCAGAAG CCACGCCCAT TAGTGAAACG CTTCATGGTG AGTTTGGATG CTGACGGACA TGTACAGGTC-**biotin**	Sangon Biotech Co., Ltd	N/A
Down 2: GACCTGTACA TGTCCGTCAG CATCCTTTTT (**T-Cy3**)TTTTTTTTT TTTTTTTTT TTTTTGTAGA GTTTCAGCAT GCACCAGAAG CCACGCCCAT TAGTGAAACG CTTCATGGTG AGTTTGGATG CTGACGGACA TGTACAGGTC-**biotin**	Sangon Biotech Co., Ltd	N/A
Down 3: GACCTGTACA TGTCCGTCAG CATCCTTTTT TTTT(**T-Cy3**)TTTTT TTTTTTTTT TTTTTGTAGA GTTTCAGCAT GCACCAGAAG CCACGCCCAT TAGTGAAACG CTTCATGGTG AGTTTGGATG CTGACGGACA TGTACAGGTC-**biotin**	Sangon Biotech Co., Ltd	N/A
Down 4: GACCTGTACA TGTCCGTCAG CATCCTTTTT TTTTTTTT(**T-Cy3**)T TTTTTTTTT TTTTTGTAGA GTTTCAGCAT GCACCAGAAG CCACGCCCAT TAGTGAAACG CTTCATGGTG AGTTTGGATG CTGACGGACA TGTACAGGTC-**biotin**	Sangon Biotech Co., Ltd	N/A
Recombinant DNA		
pET 15b expression plasmid	(Xu et al., 2003)	N/A
Software and algorithms		
Step-finding algorithm	(Kerssemakers et al., 2006)	N/A

RESOURCE AVAILABILITY

Lead contact

Further information and requests for resources and reagents should be directed to and will be fulfilled by the Lead Contact, Ying Lu (yinglu@iphy.ac.cn).

Materials availability

This study did not generate new reagents. Plasmids generated in this study are available from the Lead Contact upon request.

Data and code availability

All data needed to evaluate the conclusions in the paper are present in the paper and/or Supplemental information. Raw data were deposited on Mendeley. DOI is listed in the key resources table.

This paper does not report original code.

Any additional information required to reanalyze the data reported in this paper is available from the lead contact upon request.

EXPERIMENTAL MODEL AND SUBJECT DETAILS

E. coli strains for *in vitro* studies

The *E. coli* strain BL21 (DE3) or *E. coli* ER2566 cell (NEB) was used to express the helicase proteins. These *E. coli* cells were incubated at 37°C in LB medium for about 4 hours, and then the protein expression was induced by IPTG at 18°C for 16 hours.

METHOD DETAILS

Protein expression and purification

The human BLM (642-1290) (called hBLM-wt for simplicity), and its point mutations of R1000A, R1003A, E1008A, K1009A were expressed and purified as previously described (Guo et al., 2005; Karow et al., 1997). Briefly, they were cloned into the pET15b-SUMO vector and then expressed in *E. coli* strain BL21 (DE3). Starter cultures were grown at 37°C and induced with 0.3 mM IPTG at 18 °C for 16 hours. After their SUMO tags were cleaved with Sumo protease, they were purified by fast protein liquid chromatography (FPLC) with sequential chromatography on Ni-NTA (GE Healthcare, Chicago, IL, USA) and cation-exchange chromatography (HiTrap SP, GE Healthcare). The *Escherichia coli* RecQ helicase was expressed from pET15b-SUMO expression plasmid in *Escherichia coli* strain BL21 (DE3). After the SUMO tags were cleaved with Sumo protease, then was purified through Ni-NTA column (Teng et al., 2020). The *Gallus gallus* WRN (512-1213) helicase was expressed and purified as previously described (Wu et al., 2017). In brief, it was expressed in *E. coli* ER2566 cell (NEB) and induced with 0.3 mM IPTG at 18°C overnight. After centrifugation, WRN was purified by FPLC with sequential chromatography on Ni-NTA and Heparin (GE Healthcare). The proteins were stored at −80°C in the storage buffer.

DNA constructs and annealing procedures

All oligonucleotides required to prepare the DNA substrates were purchased from Sangon Biotech Co., Ltd (Shanghai, China), which have been purified by ULTRAPAGE. The sequences of each DNA template are described in Table S1. DNA was annealed by incubating the mixture at 95°C for 5 min and then cooling it to room temperature for approximately 7 h. The annealing was carried out with a buffer containing 50 mM NaCl and 25 mM Tris-HCl (pH 7.5 at 25°C) (Lin et al., 2017).

Single-molecule FRET assay

The smFRET study was carried out in a home-built objective-type total internal reflection fluorescence microscopy (Myong et al., 2005). Cy3 was excited by a 532 nm sapphire laser (Coherent Inc., USA). An oil immersion objective (100×, N.A. 1.49) was used to generate an evanescent field of illumination. The fluorescence signals from Cy3 and Cy5 were split by a dichroic mirror and collected by an electron-multiplying charge-coupled-device camera (iXON, Andor Technology, South Windsor, CT, USA). The coverslips (Fisher Scientific, USA) and slides were cleaned thoroughly by rinsing with acetone, methanol, a mixture of sulfuric acid and hydrogen peroxide (7:3, v/v), and sodium ethoxide. The surfaces of coverslip were coated with a mixture of 99% mPEG (methoxy-PEG-5,000, Laysan Bio, Inc.) and 1% biotin-PEG (biotin-PEG-5,000, Laysan Bio, Inc.). Streptavidin was added to the microfluidic chamber and incubated for 5 min. The chamber was made of the PEG-coated coverslip. After washing with buffer, ~100 pM DNA was added to the chamber and immobilized for 5 min. Free DNA molecules were removed by washing the chamber. Then the proteins were injected in the chamber, ATP may also add in the unwinding assays. The time resolutions were

50–250 ms. All the experiments were carried out at 25°C. At conditions without helicase, a buffer containing 20 mM Tris-HCl (pH 8.0 at 25°C) and 50 mM NaCl was used. The helicase binding and unwinding buffer contained 50 mM Tris-HCl (pH 8.0 at 25°C), 50 mM NaCl, 5 mM $MgCl_2$, and 5 mM dithiothreitol. In single-molecule FRET measurements, an oxygen-scavenging system containing 0.8% (w/w) D-glucose, 1 mg/mL glucose oxidase (266.6 units/mg, Sigma), 0.4 mg/mL catalase (2,000–5,000 units/mg, Sigma), and 1 mM Trolox was added to the helicase binding and unwinding buffer. Final concentrations were used in all cases.

QUANTIFICATION AND STATISTICAL ANALYSIS

After the local background, cross-talk, quantum yield and detection efficiency were corrected, the FRET efficiency was calculated (Roy et al., 2008). We used an unbiased step-finding algorithm developed by Kerssemakers and co-workers (Kerssemakers et al., 2006) to analysis the steps. Briefly, we fitted a single large step to the data, finding the size and location based on a calculation of a chi-square. We then searched for new steps by fitting them to the plateaus from the previous cycles, each time selecting the most prominent one. This eventually led to a series of "best" fits that differed only by a single-step. We then compared each best fit in the series to a "counter" fit that had an equal number of steps as the original one but with step locations displaced randomly. A "step-indicator" *S* defined as the ratio between the chi-square of the counter fit and the chi-square of the best fit was then used to evaluate the quality of the step fits. *S* was large when the number of steps in the best fit was close to the real number of steps. After fitting the original FRET data, the FRET of the pauses was determined. All the statistical details of experiments can be found in the figure legends.